Korean J. Chem. Eng., 32(5), 903-910 (2015)
DOI: 10.1007/s11814-014-0306-x

pISSN: 0256-1115
eISSN: 1975-7220

Hydrothermal synthesis of different morphologies of $MgFe_2O_4$ and magnetic cellulose acetate nanocomposite

Davood Ghanbari and Masoud Salavati-Niasari†

Institute of Nano Science and Nano Technology, University of Kashan, Kashan, P. O. Box 87317-51167, Iran
(*Received 27 July 2014 • accepted 8 October 2014*)

Abstract−$MgFe_2O_4$ nanostructures were synthesized via a facile hydrothermal reaction. The effect of various surfactants such as cationic, anionic and polymeric on the morphology of the product was investigated. Magnetic nanoparticles were added to cellulose acetate (CA) to make magnetic nanocomposite. Nanoparticles appropriately enhanced flame retardant property of the CA matrix. Application of the most conventional flame retardants is limited with respect to the environmental requirements. The most important novelty of this work is the preparation of a nontoxic magnetic and flame retardant cellulose acetate nanocomposite. Dispersed nanoparticles play the role of a magnetic barrier layer, which slows down product volatilization and prevents flame and oxygen from reaching the sample during decomposition of the polymer. In the presence of flame, magnetic nanoparticles remain together (show resistance to drop falling) and build a barrier. Also, distribution of the magnetic nanoparticles into cellulose acetate matrix increases the coercivity.

Keywords: Nanoparticles, Magnetic, Nanocomposite, Flame Retardancy

INTRODUCTION

Magnetic nanostructures are widely used as components in various applications of industrial and medical equipments. Ferrites have emerged as novel materials with vast technological and scientific interest considering their brilliant physical properties such as reliable magnetization, large magneto-crystalline anisotropy, remarkable chemical stability and low cost. Since their discovery in the 1950s, the degree of interest in them has grown enormously, and is still growing today. They have been used for magnetic recording, data storage materials, radar absorbing materials and magnetoelectric applications [1-6]. Ferrite materials may be classified into three different classes: spinel, garnet and hexagonal. Magnesium ferrite is one of the important magnetic oxides with spinel structure. Preparation of $MgFe_2O_4$ nanostructures is important for its novel magnetic properties, particularly super-paramagnetic behavior and biomedical applications. The eco-friendly ferrites are well known for their enormous applications in the field of magnetic and electronic materials and photo-catalytic applications. Among spinel ferrites, $MgFe_2O_4$ have been widely used in different fields such as humidity sensor and gas sensors [7-12].

In the last two decades polymer matrix nanocomposites have also been extensively investigated, since just a small amount of nanoparticles as an additive leads to production of novel high-performance materials with excellent physicochemical properties. Cellulose acetate (CA) is a well known derivative of cellulose and is widely used in a broad field of applications such as adhesive, synthetic fiber, film base in photography and separation processes (reverse osmosis and filtering) [13-16]. Various methods for improving the fire retardancy of polymers have been developed. Improvement in flame retardancy is mainly achieved by adding halogenated compounds. Flame retardation is a process by which the normal degradation or combustion of samples is changed. Most popular flame retardants produce toxic gases during the flaming reaction and are limited with respect to the environmental restrictions and health consideration. Therefore, it is important to develop a new generation of flame retardants to substitute with the current flame retardants.

We prepared different morphologies of $MgFe_2O_4$ nanostructures using hydrothermal reaction. While the predominant morphology in other methods like sol-gel, microwave and sono-chemical is nanoparticles, hydrothermal method provides preferable orientated morphology. In hydrothermal method, because of some particular conditions (high temperature and pressure), nanoparticles grow in situ and form novel extraordinary shapes [17-21]. Nanoparticles were characterized using X-ray diffraction (XRD), scanning electron microscopy (SEM), transmission electron microscopy (TEM) and atomic force microscopy (AFM). The magnetic properties of the samples were also investigated using an alternating gradient force magnetometer (AGFM). The $MgFe_2O_4$ were then added to cellulose acetate. Magnetic properties of $MgFe_2O_4$ nanoparticles and nanocomposites were also compared. Results confirmed nanoparticles appropriately enhanced flame retardant property of the CA matrix.

EXPERIMENTAL

1. Materials and Methods

$Fe(NO_3)_3$ $9H_2O$ and $Mg(NO_3)_2$ $6H_2O$, NaOH and acetone were purchased from Merck Company. All the chemicals were used as received without further purifications. XRD patterns were recorded by a Philips, X-ray diffractometer using Ni-filtered CuK_α radiation.

†To whom correspondence should be addressed.
E-mail: Salavati@kashanu.ac.ir

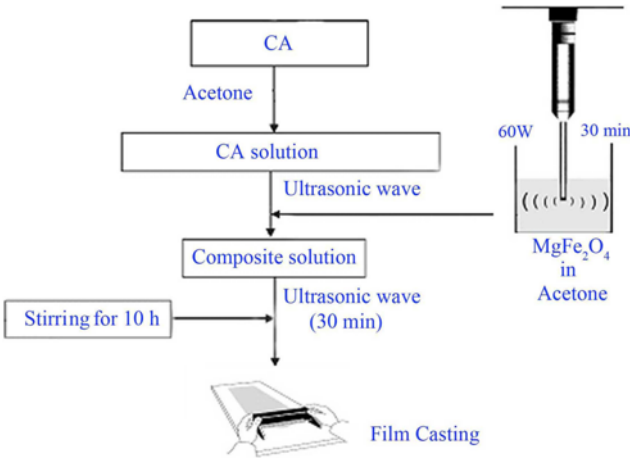

Fig. 1. Schematic of preparation of nanocomposite.

A multi-wave ultrasonic generator (Bandeline MS 72), equipped with a converter/transducer and titanium oscillator, operating at 20 kHz with a maximum power output of 76 W was used for the

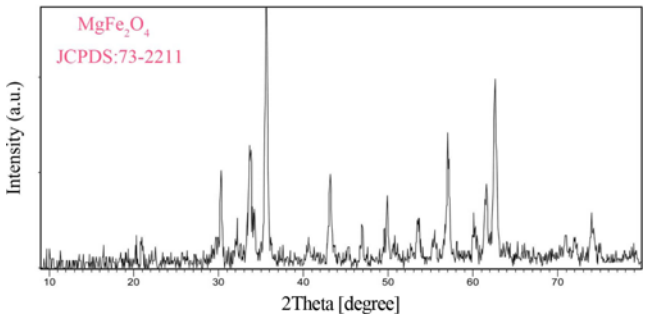

Fig. 2. XRD pattern of $MgFe_2O_4$ nanoparticles.

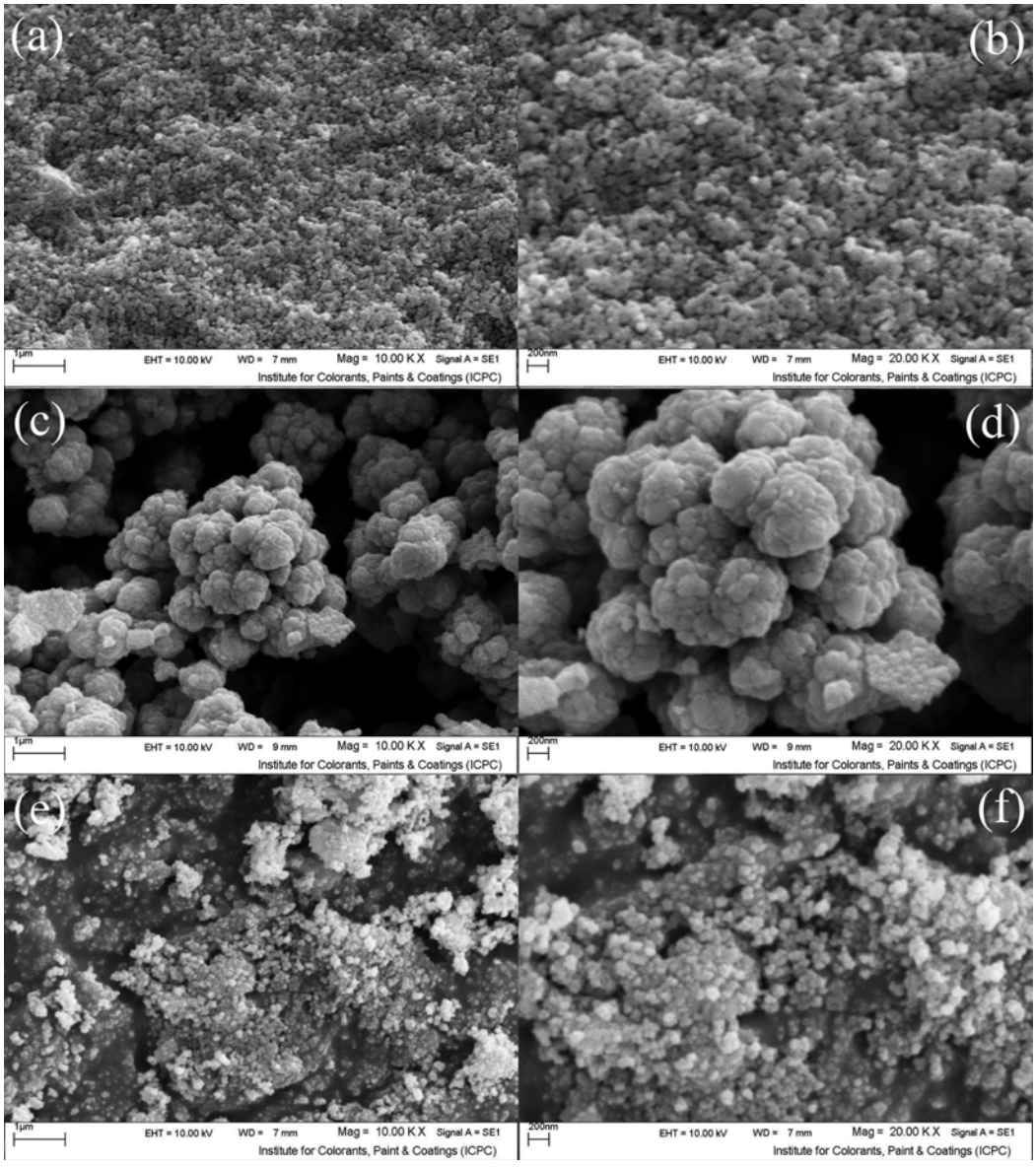

Fig. 3. SEM images of nanostructures obtained by (a), (b) CTAB (c), (d) SDS and (e), (f) without surfactant.

ultrasonic irradiation. SEM images were obtained using a LEO instrument model 1455VP. Prior to taking images, the samples were coated by a very thin layer of Pt (using a BAL-TEC SCD 005 sputter coater) to make the sample surface conductor and prevent charge accumulation, and obtaining a better contrast. Room temperature magnetic properties were investigated using an alternating gradient force magnetometer (AGFM) device, made by Meghnatis Daghigh Kavir Company in an applied magnetic field sweeping between ±10,000 Oe. In UL-94 a bar shape sample 130×13×1.6 mm is held vertically. A Bunsen burner flame is applied to the specimen twice (10 s each).

2. Synthesis of $MgFe_2O_4$ Nanoparticles

$Mg(NO_3)_2$ $6H_2O$ (0.001 mol), $Fe(NO_3)_3$ $9H_2O$ (0.002 mol) and 0.7 g of surfactant were dissolved in 190 mL of distilled water. 10 mL of NaOH solution 1 M was then slowly added to the solution. The reactants were then put into a Teflon-lined autoclave of 500 ml capacity. The autoclave was maintained at 160 °C for 6 h. The black product was centrifuged, washed with distilled water and dried in the air. The powders obtained in this stage were then calcined at 500 °C for 2 hours.

3. Preparation of Nanocomposite

4 g of cellulose acetate was first dissolved in 10 ml acetone solution. 1 g of nanoparticles $MgFe_2O_4$ was dispersed in 10 ml acetone solution with ultrasonic waves (30 min, 60 W). The nanoparticles dispersion was then slowly added to the polymer solution. The new solution was then mixed and stirred for 10 hours. In order to evaporate the solvent, the product was cast on a piece of glass template and left for 24 hours (Fig. 1).

RESULTS AND DISCUSSION

XRD pattern of $MgFe_2O_4$ nanoparticles (calcined at 500 °C) is shown in Fig. 2. The pattern of as-prepared nanoparticles is indexed as a pure cubic phase (space group: Fd-3m), which is very close to the literature values (JCPDS No. 73-2211). Results show without calcination and in lower temperatures (<500 °C) crystallite phase of ferrite was not obtained appropriately.

The crystallite size measurements were also carried out using the Scherrer equation, $Dc=K\lambda/\beta Cos\theta$, where β is the width of the observed diffraction peak at its half maximum intensity (FWHM), K is the so-called shape factor, which usually takes a value of about 0.9, and λ is the X-ray wavelength (CuK_α radiation, equals to 0.154 nm). The estimated crystallite size is about 28 nm.

The effect of cationic and anionic surfactant on the morphology of the product was investigated. By using cethyl tri-methyl ammonium bromide (CTAB: cationic surfactant) nanoparticles with average diameter of 30 nm were obtained (Fig. 3(a) and 3(b)). It shows nucleation stage overcome to growth stage, and therefore nanoparticles were achieved. Fig. 3(c) and 3(d) show SEM images of the product when sodium dodecyl sulphate (SDS: anionic surfactant) was used that confirm nanostructures were synthesized. SDS leads to preferential growth in nanoparticles and as a result nanostructures were obtained. With applying SDS, the magnetic product must be washed completely in order to prevent the formation of metal-sulfur impurity. While CTAB has an advantage compared to SDS because it totally decomposes and evaporates in calcination at 500 °C. Blank reaction was also performed for mak-

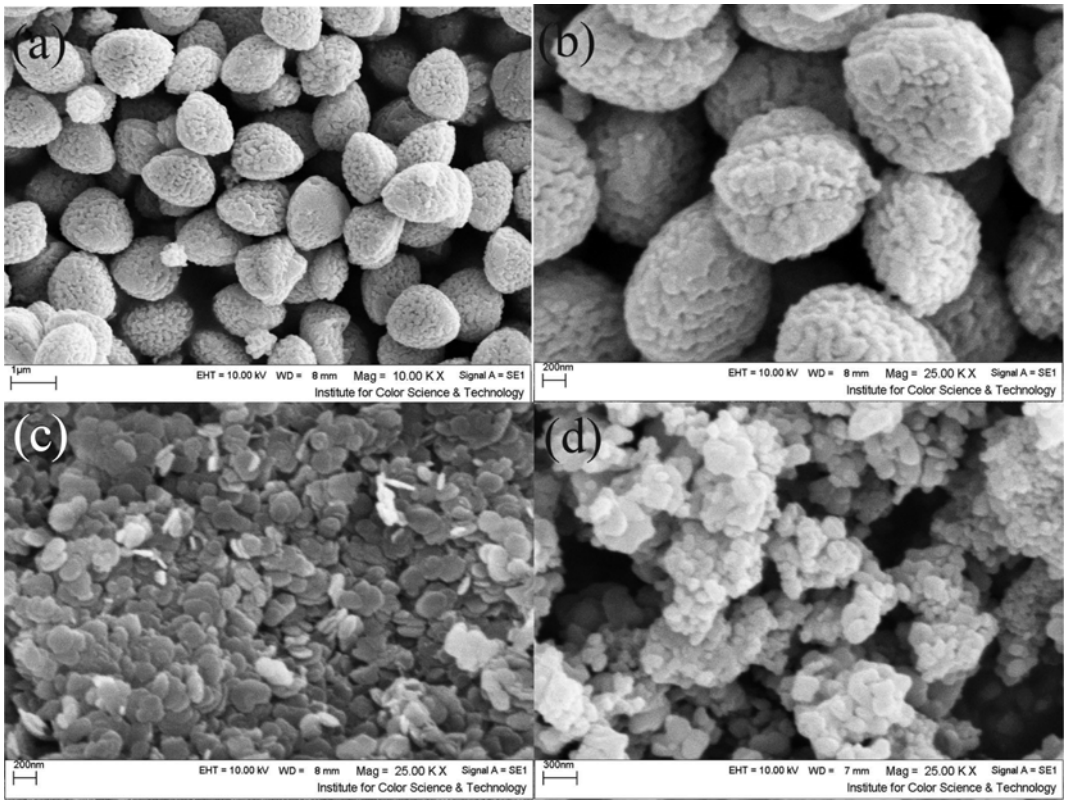

Fig. 4. SEM images of nanostructures prepared with (a), (b) PVP, (c) PVA and (d) PEG.

ing better comparison and results confirm without using surfactants (CTAB and SDS) some agglomeration was observed that are shown in Fig. 3(e)-(f).

The polymers' influence (neutral surfactants) on the particle size and shape of the nanostructures were examined. Three kinds of water soluble polymers were chosen for hydrothermal reaction. By using polyvinyl pyrrolidone (PVP: MW25000) porous-nanostructures were obtained that are illustrated in Fig. 4(a) and 4(b). SEM images show preferential growth by applying PVP, which means growth stage has been preferred compared to nucleation stage, and as a result porous-nanostructures were synthesized. Fig. 4(c) shows the product when poly vinyl alcohol (PVA: MW20000-30000) was used and plate-like nanostructures were synthesized. By applying polyethylene glycol (PEG: MW6000) amorphous nanostructures were achieved (Fig. 4(d)).

TEM images of nanoparticles obtained by CTAB are illustrated

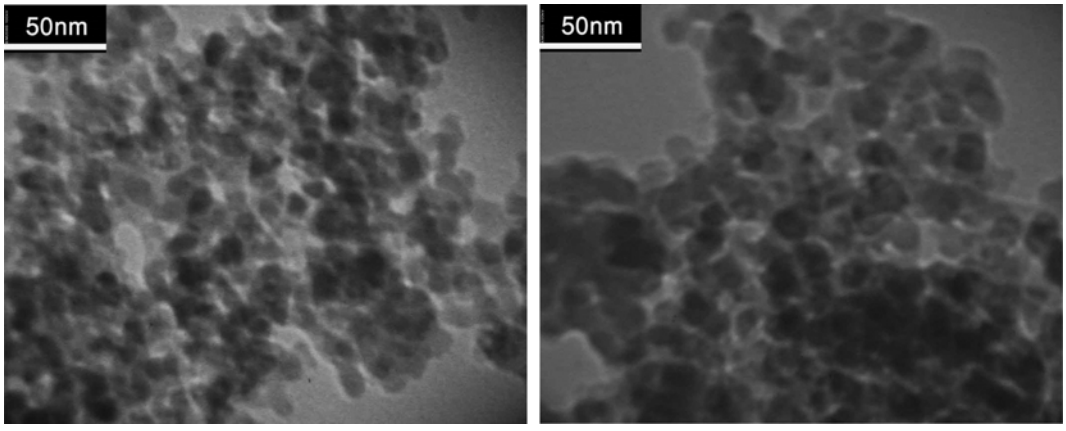

Fig. 5. TEM images of nanoparticles obtained by CTAB.

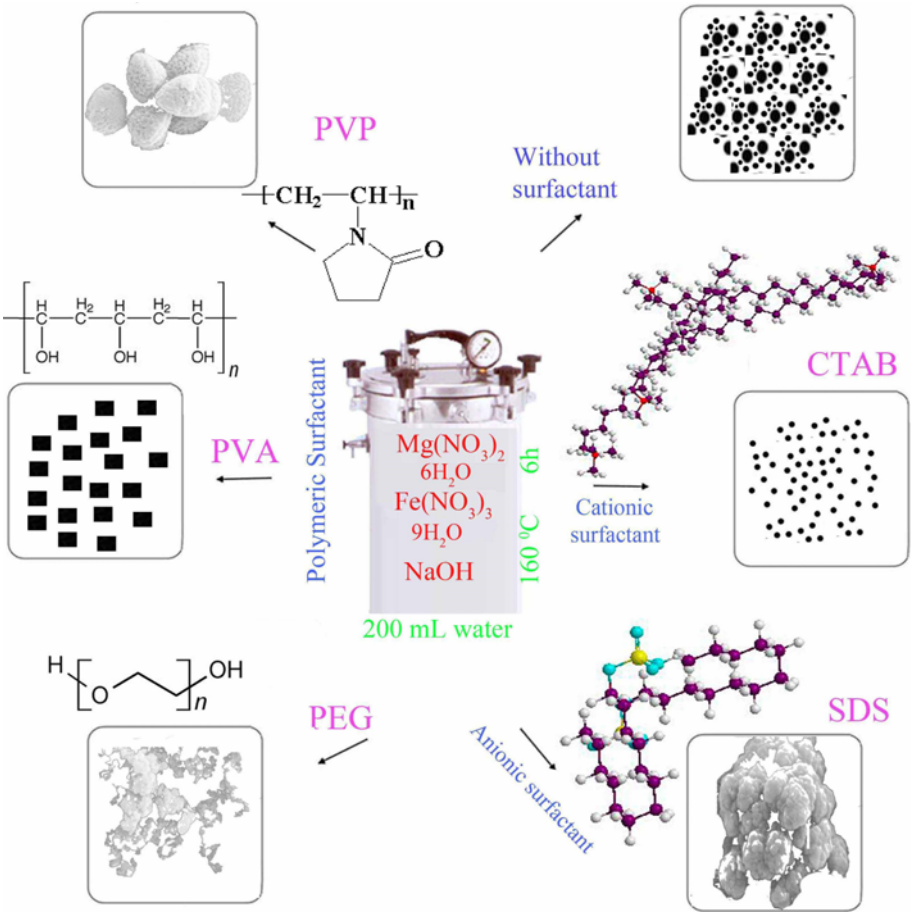

Fig. 6. Effect of various surfactants on the morphology of $MgFe_2O_4$ nanostructures.

in Fig. 5 that shows nanoparticles with average diameter of 15 nm.

In hydrothermal method, because of high temperature and pressure, nanoparticles grow in situ and form novel shapes [17-21]. Formation of $MgFe_2O_4$ and surfactant effect on the shape is depicted in Fig. 6 schematically.

Fig. 7(a) shows SEM image of the pure cellulose acetate surface that shows flat surface of cellulose acetate. There are some cracks in the surface because CA decomposes slightly under electron beam. Fig. 7(b) and 7(c) show SEM images of CA-$MgFe_2O_4$ nanocomposite that confirms the appropriate dispersion of nanoparticles in the cellulose acetate matrix.

Topographic AFM plot of pure cellulose acetate and CA-$MgFe_2O_4$

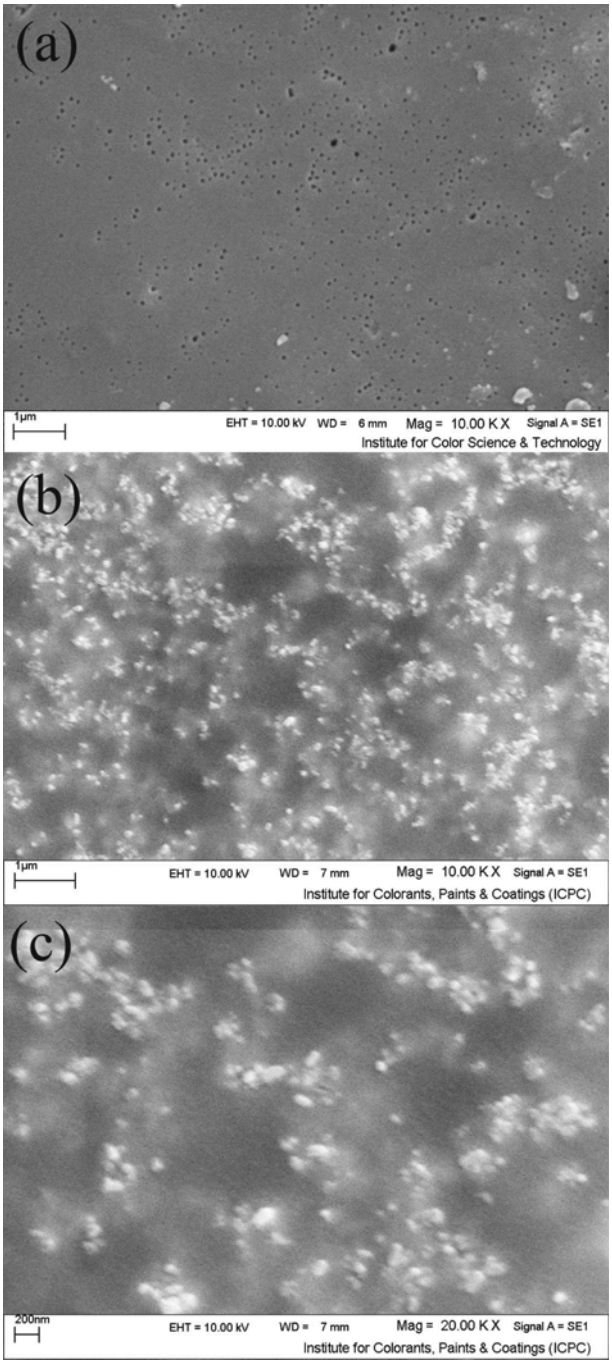

Fig. 7. SEM images of (a) pure CA and (b), (c) CA-$MgFe_2O_4$ nanocomposite.

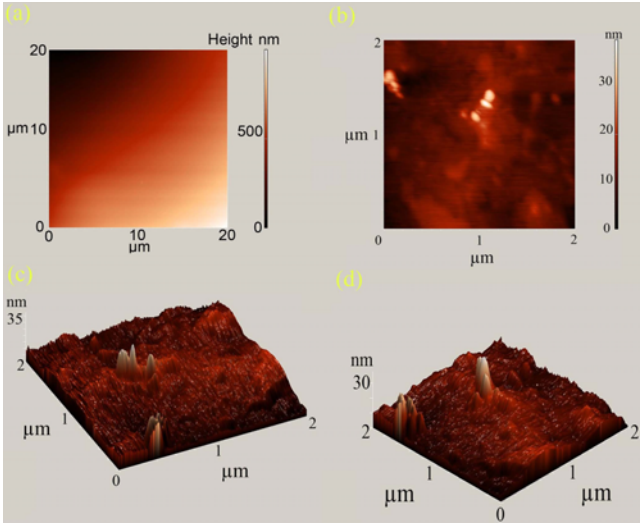

Fig. 8. AFM images of (a) pure CA and (b), (c), (d) CA-$MgFe_2O_4$ nanocomposite.

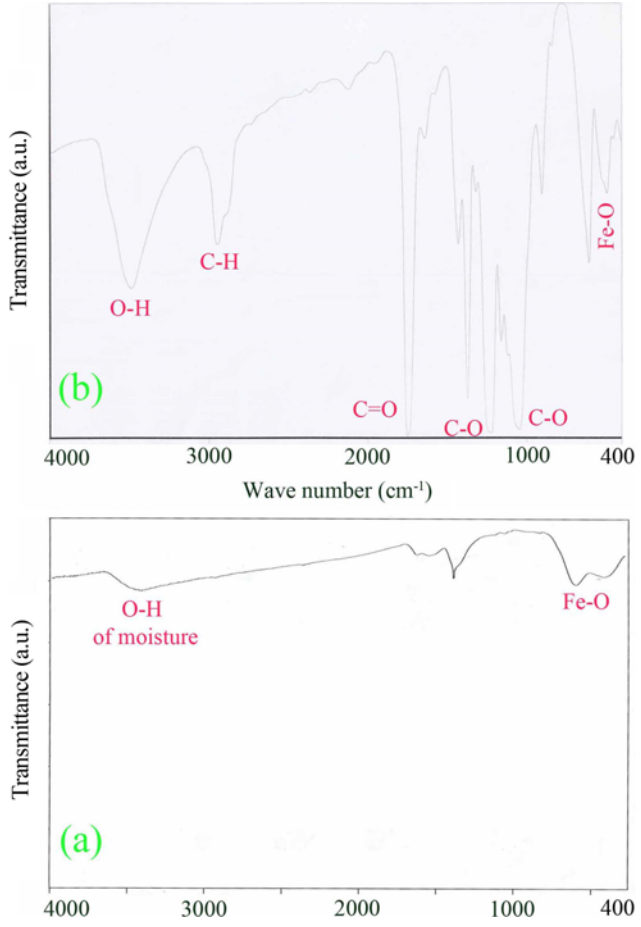

Fig. 9. FT-IR spectra of (a) $MgFe_2O_4$ nanoparticles (b) CA-$MgFe_2O_4$ nanocomposite.

is shown in Fig. 8. Pure polymer shows smooth surface (Fig. 8(a)). Roughness in the surface of the nanocomposite approves the presence of the nanostructures in the polymeric matrix (Fig. 8(b)-(d)).

FT-IR spectrum of $MgFe_2O_4$ nanoparticles is depicted in Fig. 9(a). Absorptions at 414 cm^{-1} and 596 cm^{-1} are related to Fe-O bonds in nanoparticles, and absorption in 3,414 cm^{-1} is responsible for O-H bonds (moisture) that adsorbed on the surface of the nanoparticles. There is no strong peak related to precursors (nitrates, surfactants) that shows pure nanoparticle was synthesized. Fig. 9(b) is the FT-IR spectrum of CA-$MgFe_2O_4$ nanocomposite; a peak at 1,751 cm^{-1} is related to the C=O bond in CA. Absorptions at 1,044 and 1,161 cm^{-1} are attributed to the C-O bonds in CA polymer. Peak at 3,486 cm^{-1} refers to the stretching vibration of O-H bond [21]. Absorption at 414 cm^{-1} at nanocomposite confirms existence of the $MgFe_2O_4$ in the cellulose acetate matrix.

Room temperature magnetic properties of our samples were studied using an AGFM device. Hysteresis loop for $MgFe_2O_4$ nanoparticles is shown in Fig. 10. It was found that the as-obtained $MgFe_2O_4$ nanoparticles exhibit ferrimagnetic behavior with a saturation magnetization of 24.4 emu/g, a coercivity of 87 Oe and magnetization remanent of 4.97 emu/g that is compatible to previous published papers reporting magnetization and coercivity.

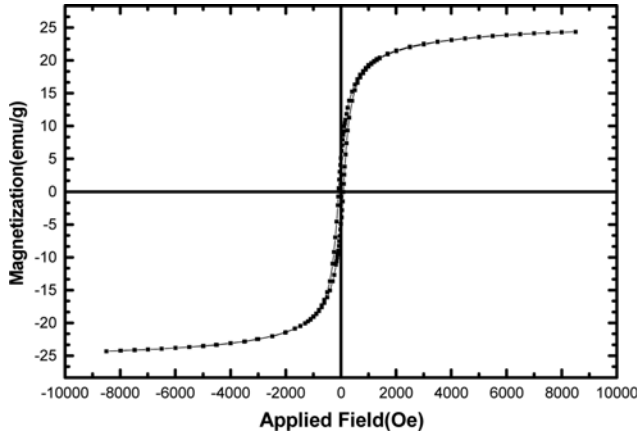

Fig. 10. Room temperature hysteresis loop of $MgFe_2O_4$ nanoparticles.

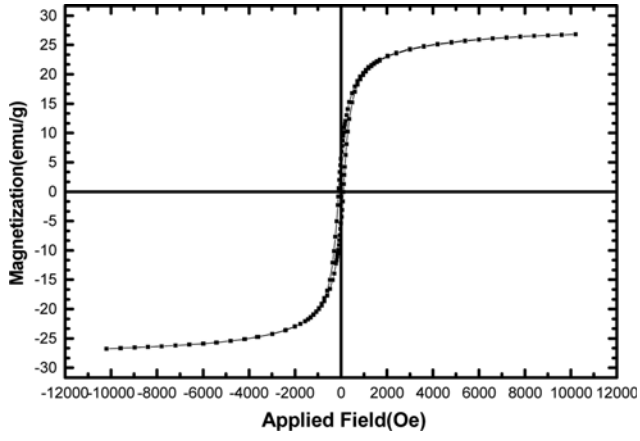

Fig. 11. Hysteresis loop of $MgFe_2O_4$ porous nanostructures.

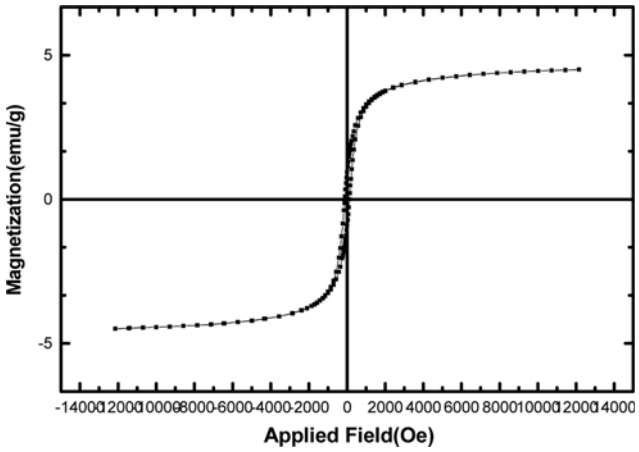

Fig. 12. Hysteresis loop of CA-$MgFe_2O_4$ nanocomposite.

Fig. 11 illustrates loop of porous-nanostructure. Nanostructures have a ferrimagnetic characteristic with a saturation magnetization of 26.8 emu/g and a coercivity of 101 Oe. Because the size of magnetic domains increases in porous nanostructures, coercivity is higher than that of nanoparticles.

A hysteresis graph for CA-$MgFe_2O_4$ nanocomposite is illustrated in Fig. 12. Nanocomposite presents a saturation magnetization of 4.6 emu/g and a coercivity of 122 Oe.

To our best knowledge and based on our search in the literature, very little work has been done on magnetic cellulose acetate nanocomposites. We studied the magnetic interaction between the nanoparticles surrounded by the polymeric chains. This interaction leads to an increase (from 87 to 122 Oe) of nanoparticle coercivities compared with the pure magnesium ferrite nanoparticles.

A possible explanation for this result could be as follows: The magnetic moments of magnetic nanoparticles are pinned by the cellulose acetate matrix chains, so that a higher magnetic field is required for aligning the single domain nanoparticles in the field direction [3,21]. This effect is illustrated in Fig. 13 schematically.

To make 5 g magnetic nanocomposite, 1 g of ferrite nanoparticles is added to 4 g of polymer. Thus the nanocomposite magnetization (defined as the magnetic moment per unit volume) is about one-fifth of which is obtained for $MgFe_2O_4$ nanoparticles.

The saturation magnetization of nanoparticles is higher than that is obtained for CA-$MgFe_2O_4$ nanocomposites. Coercivity of magnetic nanocomposites highly depends on the magnetic nanoparticle distribution into the polymeric matrix. Coercivity, remanence and saturation magnetization of the synthesized samples are listed in Table 1.

The influence of $MgFe_2O_4$ on the flame retardancy has been considered using UL-94 test.

If sample is extinguished in less than 10 seconds after any flame application classified as V-0, drips of particles are allowed as long as they are not inflamed. A V-1 classification is given to a sample with maximum combustion time less than 30 seconds; circumstances of drips are like V-0. The sample is classified V-2 if it has the combustion time criterion of V-1, but flaming drips are allowed. Samples are ranked as N.C. in UL-94 tests when the maximum total flaming time is above 50 s. The sample is classified HB when slow burning on a horizontal specimen, burning rate less than 76 mm/

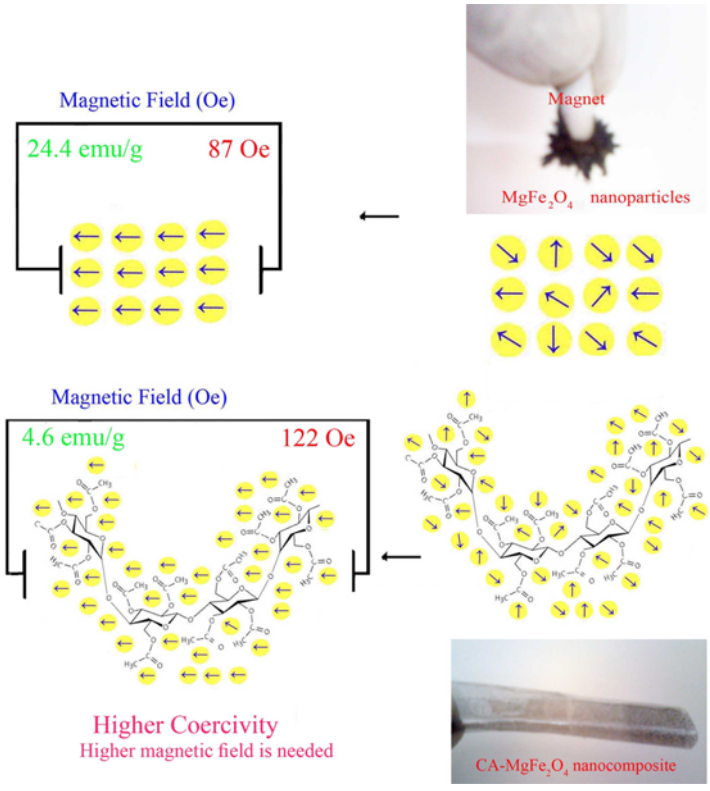

Fig. 13. Schematic illustration of $MgFe_2O_4$ nanoparticles and distributed nanoparticles in polymer matrix in absence and presence of a magnetic field.

Table 1. Coercivity, remanence and saturation magnetization of the $MgFe_2O_4$ nanostructures and nanocomposite

Sample	Saturation magnetization (emu/g)	Coercivity (Oe)	Remanence (emu/g)
$MgFe_2O_4$ nanoparticle	24.4	87	4.97
$MgFe_2O_4$ porous-like	26.8	101	5.52
CA-$MgFe_2O_4$	4.6	122	0.92

min [3,21].

The outcomes of UL-94 tests for CA and CA-$MgFe_2O_4$ are N.C and V-0, respectively. The results show that the $MgFe_2O_4$ can enhance the flame retardancy of the CA matrix. According to the UL-94 test, nanoparticles have been appropriately interacting in CA matrix. Comparison of pure CA and CA-$MgFe_2O_4$ nanocomposite under UL-94 test is shown in Fig. 14.

Hydroxyl groups on the surface of ferrite have suitable interaction with hydroxyl and carbonyl groups of cellulose acetate. Because of the mentioned interaction, nanoparticles are appropriately dispersed in polymer matrix. In the presence of flame and occurrence of polymer decomposition, magnetic nanoparticles remain together. This obstruction resists dropping, delays evaporation of polymeric segments and prevents reaching oxygen and flame to the sample.

CONCLUSIONS

Various morphologies of $MgFe_2O_4$ nanostructures were prepared

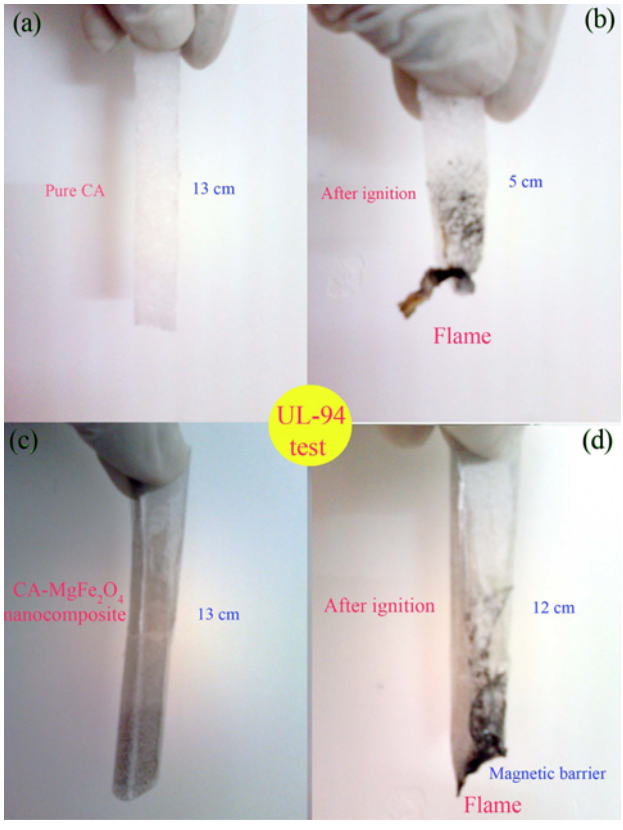

Fig. 14. Comparison of (a), (b) pure CA and (c), (d) CA-$MgFe_2O_4$ nanocomposite under UL-94 test.

via a hydrothermal reaction. The influence of different surfactants such as CTAB, SDS and polymeric on the morphology of the product was examined. Nanoparticles exhibit a ferrimagnetic behaviour with a saturation magnetization of 24.4 emu/g and a coercivity of 87 Oe at room temperature. For fabricating magnetic nanocomposites, nanoparticles were added to CA polymeric matrix. The coercivity increased as result of $MgFe_2O_4$ distribution in the cellulose acetate matrix. The results show that magnetic obstruction can enhance the flame retardancy of the CA matrix.

ACKNOWLEDGEMENTS

Authors are grateful to the council of university of Kashan for their unending effort to provide financial support to undertake this work by Grant No (159271/205).

REFERENCES

1. M. Pal, S. Bid, S. K. Pradhan, B. K. Nath, D. Das and D. Chakravorty, *J. Magn. Magn. Mater.*, **269**, 42 (2004).
2. R. C. Pullar, I. K. Bdikin and A. K. Bhattacharya, *J. Eur. Ceram. Soc.*, **32**, 905 (2012).
3. D. Ghanbari, M. Salavati-Niasari and M. Ghasemi-Kooch, *J. Ind. Eng. Chem.*, **20**, 3970 (2014).
4. M. Cernea, S.-G. Sandu, C. Galassi, R. Radu and V. Kuncser, *J. Alloys Compd.*, **561**, 121 (2013).
5. D. Lisjak and M. Drofenik, *J. Eur. Ceram. Soc.*, **26**, 3681 (2006).
6. U. Topal, H. Ozkan and H. Sozeri, *J. Magn. Magn. Mater.*, **284**, 416 (2004).
7. S. Verma, P. A. Joy, Y. B. Khollam, H. S. Potdar and S. B. Deshpande, *Mater. Lett.*, **58**, 1092 (2004).
8. Y. Shen, Y. Wu, X. Li , Q. Zhao and Y. Hou, *Mater. Lett.*, **96**, 85 (2013).
9. Y. Huang, Y. Tang, J. Wang and Q. Chen, *Mater. Chem. Phys.*, **97**, 394 (2006).
10. C. Gong, Y.-J. Bai, Y.-X. Qi, N. Lun and J. Feng, *Electrochim. Acta*, **90**, 119 (2013).
11. Z. Durmus, B. Unal, M. S. Toprak, A. Aslan and A. Baykal, *Phys. B.*, **406**, 2298 (2011).
12. B. Unal, Z. Durmus, A. Baykal, M. S. Toprak, H. Sozeri and A. Bozkurt, *J. Alloy Compd.*, **509**, 8199 (2011).
13. Z. Durmus, H. Kavas, H. Sozeri, M. S. Toprak, A. Aslan and A. Baykal, *J. Supercond. Nov. Magn.*, **25**, 1185 (2012).
14. F. Gholamian, M. Salavati-Niasari, D. Ghanbari and M. Sabet, *J. Clust. Sci.*, **24**, 73 (2013).
15. P. Jamshidi, D. Ghanbari and M. Salavati-Niasari, *J. Ind. Eng. Chem.*, **20**, 3507 (2014).
16. M. Yousefi, E. Noori, D. Ghanbari, M. Salavati-Niasari and T. Gholami, *J. Clust. Sci.*, **25**, 397 (2014).
17. D. Ghanbari, M. Salavati-Niasari and M. Sabet, *Compos. Part B Eng.*, **45**, 550 (2013).
18. A. Sobhani and M. Salavati-Niasari, *Mater. Res. Bull.*, **53**, 7 (2014).
19. A. Sobhani and M. Salavati-Niasari, *Superlattice Microstruct.*, **65**, 79 (2014).
20. A. Sobhani and M. Salavati-Niasari, *Mater. Res. Bull.*, **48**, 3204 (2013).
21. D. Ghanbari and M. Salavati-Niasari, *J. Ind. Eng. Chem.*, In Press (2014).